Published in final edited form as:
Am J Physiol Cell Physiol. 2008 March ; 294(3): C743–C753. doi:10.1152/ajpcell.00250.2007.

Two-dimensional kinetics of β_2-integrin and ICAM-1 bindings between neutrophils and melanoma cells in a shear flow

Shile Liang[1,*], **Changliang Fu**[2,*], **Desiree Wagner**[1], **Huiguang Guo**[2], **Dongying Zhan**[2], **Cheng Dong**[1], and **Mian Long**[2]

1*Department of Bioengineering, The Pennsylvania State University, University Park, Pennsylvania*

2*National Microgravity Laboratory and Center for Biomechanics and Bioengineering, Institute of Mechanics, Chinese Academy of Sciences, Beijing, People's Republic of China*

Abstract

Cell adhesion, mediated by specific receptor-ligand interactions, plays an important role in biological processes such as tumor metastasis and inflammatory cascade. For example, interactions between β_2-integrin (lymphocyte function-associated antigen-1 and/or Mac-1) on polymorphonuclear neutrophils (PMNs) and ICAM-1 on melanoma cells initiate the bindings of melanoma cells to PMNs within the tumor microenvironment in blood flow, which in turn activate PMN-melanoma cell aggregation in a near-wall region of the vascular endothelium, therefore enhancing subsequent extravasation of melanoma cells in the microcirculations. Kinetics of integrin-ligand bindings in a shear flow is the determinant of such a process, which has not been well understood. In the present study, interactions of PMNs with WM9 melanoma cells were investigated to quantify the kinetics of β_2-integrin and ICAM-1 bindings using a cone-plate viscometer that generates a linear shear flow combined with a two-color flow cytometry technique. Aggregation fractions exhibited a transition phase where it first increased before 60 s and then decreased with shear durations. Melanoma-PMN aggregation was also found to be inversely correlated with the shear rate. A previously developed probabilistic model was modified to predict the time dependence of aggregation fractions at different shear rates and medium viscosities. Kinetic parameters of β_2-integrin and ICAM-1 bindings were obtained by individual or global fittings, which were comparable to respectively published values. These findings provide new quantitative understanding of the biophysical basis of leukocyte-tumor cell interactions mediated by specific receptor-ligand interactions under shear flow conditions.

Keywords

heterotypic cell aggregation; adhesion molecule; leukocyte; tumor cell; reverse rate; binding affinity; probabilistic model; polymorphonuclear neutrophils; intercellular adhesion molecule-1

MELANOMA IS HIGHLY MALIGNANT in forming metastasis. Most deaths from melanoma are due to metastases that are resistant to conventional therapies (35,39). Tumor metastasis consists of a complex cascade, in which the adhesion to and subsequent extravasation through the vascular endothelium (EC) is a critical step. Human polymorphonuclear neutrophils (PMNs), which comprise 50 −70% of circulating leukocytes, have been shown to promote tumor adhesion and transendothelial extravasation under certain circumstances (18,37,48). Aggregation between melanoma cells and PMNs in blood vessels is regulated by underlying interacting molecules

Address for reprint requests and other correspondence: C. Dong, Dept. of Bioengineering, The Pennsylvania State Univ., University Park, PA 16802−6804 (e-mail: E-mail: cxd23@psu.edu)..

*S. Liang and C. Fu contributed equally to this work.

under shear conditions. For example, it has been recently reported that binding between ICAM-1 on malignant melanoma cells and β_2-integrins [e.g., CD11a/CD18 or lymphocyte function-associated antigen-1 (LFA-1), CD11b/CD18 or Mac-1] on PMNs mediates melanoma extravasation through the EC (18,37). ICAM-1 is a member of the immunoglobulin (IgG) super family, which is composed of five extracellular IgG domains with a transmembrane domain and a cytoplasmic tail and expresses with a dose- and time-dependent increase in human malignant melanoma cells on stimulation of TNF-α (27). Inhibition of ICAM-1 expression on melanoma cells reduces the metastatic ability of the melanoma cells (27), indicating an important role of ICAM-1 in metastasis. β_2-Integrin is a heterodimeric molecule that consists of α- and β-subunits with an extracellular domain, a transmembrane domain, and a cytoplasmic tail. β_2-Integrin on PMNs has been shown to be upregulated on stimulation of chemoattractant, which is essential for PMNs to form firm adhesion to the EC and subsequent migration to the surrounding tissue in response to inflammation (2,40).

Cellular aggregation kinetics has been extensively investigated in the past decades. For example, the heterotypic aggregation between transfected cells (or beads) expressing ICAM-1 and PMNs in a shear flow has been quantified in terms of cell adhesion or capture efficiency, suggesting that the adhesion of PMNs to ICAM-1-expressing cells is a cooperative and sequential process of LFA-1-dependent initial endothelial capture of PMNs followed by Mac-1-mediated stabilization (12,28) and that the aggregation is upregulated by chemotactic stimulation with a high-affinity conformation of active CD18 (25). Such shear-induced aggregations have also been observed experimentally from the interactions between PMNs and colon carcinomas expressing ICAM-1 and sialylated molecules (15,16); the doublet formation and breakage of red cells and of latex spheres crossed-linked by antigen-antibody bonds (17, 44,45); the homotypic aggregation of PMNs mediated by L-selectin and β_2-integrin adhesion receptors (43); the heterotypic aggregation of PMNs and cells transfected with ICAM-1 (12, 26,28), E- or L-selectin (26); or PMNs and platelets or beads coated with P-selectin glycoprotein ligand 1 (PSGL-1; 26) or ICAM-1 (33). All of these observations provide an increasing recognition in cellular aggregation kinetics, which is crucial to many biological processes such as tumor metastasis, inflammatory cascade, and thrombus formation. However, cellular aggregation kinetics has rarely been correlated to the intrinsic molecular kinetics of underlying interacting molecules, especially in tumor cell adhesion.

To mediate aggregations between melanoma cells and PMNs, both ICAM-1 and β_2-integrin molecules must be anchored onto two apposing surfaces, which is called two-dimensional (2D) interaction. 2D kinetics of β_2-integrin and ICAM-1 bindings governs how likely or strongly they bind and how long they remain bound, which consequently determine the dynamic aggregations between cells. This is different from three-dimensional (3D) binding in which at least one of the receptors and ligands is in a fluid phase. In previous studies, a deterministic kinetic model upon bulk chemistry, combined with two-body collision theory (38), was proposed to predict the forward- and reverse-rates of β_2-integrin and L-selectin for PMN aggregation (42) and of GPIIb/IIIa integrin for platelet aggregation (41). A similar deterministic model was also used to estimate the cellular reverse rate of β_2-integrin and L-selectin for PMN aggregation (29). To further understand the molecular mechanism that determines the cellular aggregation kinetics, a 2D probabilistic kinetic model would be required since the 2D receptor-ligand binding is no longer a deterministic but a stochastic process (6, 13,47). In addition, the 2D kinetics should be coupled to the mechanics of receptor-ligand binding since the external forces exerted by shear flow regulate the bond formation and dissociation (4).

We have previously developed a probabilistic kinetic model to predict shear-induced doublet formations and breakages of red cells and of latex spheres crossed-linked by antigen-antibody bonds and to estimate the intrinsic forward- and reverse-rates by fitting the data with the model

(24). Here we extended that model to predict aggregations between chemotactically stimulated PMNs and melanoma cells mediated by β_2-integrin and ICAM-1 bindings. A cone-plate viscometer was used to provide a uniform shear-flow field, and flow cytometry was employed to measure the cell aggregation. The effects of hydrodynamic shear stresses, shear rates, and β_2-integrin and ICAM-1 expressions were determined experimentally. Best-fitting the data with the proposed model predicted the intrinsic kinetic rates and binding affinity of interacting β_2-integrin-ICAM-1 pairs between PMNs and melanoma cells.

MATERIALS AND METHODS

Cell preparations and reagents

WM9 melanoma cells (kindly provided by Dr. M. Herlyn, Wistar Institute, Philadelphia, PA) were grown in RPMI-1640 (Invitrogen, Carlsbad, CA) supplemented with 10% fetal bovine serum (Invitrogen). Before each experiment, WM9 cells were detached when confluent using trypsin/versine (Invitrogen) and were washed twice with fresh medium. Then the cells were resuspended in fresh medium and allowed to recover for 1 h while being rocked at 8 rpm at 37°C. For ICAM-1 blocking experiments, WM9 cells were treated with anti-ICAM-1 monoclonal antibodies (mAbs) (R&D Systems, Minneapolis, MN) for 1 h at 37°C. To upregulate the ICAM-1 expression, WM9 cells were incubated at various concentrations of tumor necrosis factor (TNF-α; Sigma) for 24 h. After stimulation, WM9 cells were spun down and resuspended in fresh media for use.

Following the Pennsylvania State University Institutional Review Board approved protocols (no. 19311), fresh human blood samples were collected from healthy donors by venipuncture. PMNs were isolated using a Histopaque (Sigma, St. Louis, MO) density gradient according to the manufacturer's instruction and were kept at 4°C in Dulbecco's PBS containing 0.1% human serum albumin for up to 4 h before use. To upregulate the expression of β_2-integrin, PMNs were incubated with 1 μM formyl-methionyl-leucyl-phenylalanine (fMLP; Sigma) for 2 min. For blocking experiments, fMLP-stimulated PMNs were pretreated for 30 min at 4°C with anti-CD11a and anti-CD11b mAbs (Invitrogen) at 5 μg/10^6 cells.

Determination of aggregation

To measure the interactions between PMNs and WM9 cells, heterotypic aggregation assays were performed in a cone-plate viscometer, which consists of a stationary plate placed beneath a rotating cone (1° angle) maintained at 37°C (RotoVisco 1; Haake, Newington, NH). Mixed suspensions of PMNs and WM9 cells, respectively prelabeled with LDS-751 (red) and tetramethylrhodamine isothiocyanate (TRITC; orange), were placed on the plate at the concentration ratio of 1:1 (10^6 cells/ml, 500 μl each cell type) and were allowed to equilibrate for 1 min. Thereafter, the heterotypic cell suspensions were stimulated with 1 μM fMLP for 2 min before the application of shear. Exposure of cell suspensions to a linear velocity gradient resulted in collisions between the faster moving cells near the rotating cone and the slower moving cells near the stationary plate (12). Shear rate, G, was varied from 62.5 to 800 s^{-1} (typically for the microcirculation) (46) for preset shear duration, t, ranging from 30 to 300 s. To understand the dependence of PMN-melanoma aggregation on shear rate and shear stress, different effects of shear stress (τ) and shear rate (G) were separated by using dextran (MW 2 × 10^6, Sigma) to vary the media viscosity, η, so that shear stress ($\tau = \eta G$) can be held constant while shear rate changes, or vice versa. After shear, aliquots were immediately fixed with 1% formaldehyde at room temperature and were subsequently analyzed with the Guava Personal Cytometer (Guava Technologies, Burlingame, CA). The size distribution and cellular composition of aggregates generated in the cone-plate viscometer were determined by a two-color flow cytometric methodology that was published (28), in which PMNs and WM9 cells were labeled with different fluorescence dyes so that the PMNs and WM9 population could

be isolated by gating on their characteristic forward versus side scatter. The heterotypic aggregation was quantified by analyzing the dot plot between the red (due to LDS-751) and the orange (due to TRITC) fluorescence channels (Fig. 1*A*). Heterotypic aggregation was quantified as the percentage of bound WM9 cells to PMNs in total WM9 cells:

$$\%\text{Tumor cells in heterotypic aggregation} = \frac{\text{number of tumor cells in aggregation}}{\text{total number of tumor cells}} \times 100\% \quad (1)$$

The statistical significance of the difference between heterotypic aggregation fractions of PMN-WM9 pairs in different shear rates and shear stresses with different chemotactic simulations was assessed with Student's *t*-test.

Probabilistic kinetic modeling

The mathematical model used here is based on the probability (P_a) of adhesion per two-body collision. This is a measure of the likelihood that a receptor-expressing cell will adhere to a ligand-expressing cell when the two collide. For shear-induced experiments in which cells experience a extremely short encounter duration, $\langle t \rangle$(specifically $\langle t \rangle = 0.86\pi/G \approx 0.043$~$0.003$ s under the experimental shear rate G) (1,26,34). We have previously shown that two cells are most likely linked by only one bond initially (24), such that $P_a \approx A_c m_r m_l k_f \langle t \rangle$. Here A_c is the contact area of the two cells; m_r and m_l are the respective site densities of receptor and ligand; k_f is the forward rate of the receptor-ligand pair; and $A_c m_r m_l k_f$ is the effective forward rate. For heterotypic aggregation in a Couette flow, the total collision frequency per unit volume H_c is determined by the cell concentrations C_1 (e.g., melanoma cells) and C_2 (e.g., PMNs), the shear rate G, and the cell radii r_1 and r_2; specifically, $H_c = 4(r_1 + r_2)^3 GC_1C_2/3$ (38). Thus, the probability of doublets formed per unit time per melanoma cell, P_p, follows $P_p = H_c P_a/C_1 = 1.15\pi(r_1 + r_2)^3 C_2 A_c m_r m_l k_f$. Once a doublet forms, more bonds may form or the existing bonds may break in the remaining shear duration. This bond evolution is modeled here by using the equations of a previously developed probabilistic model (24):

$$dp_n/dt = A_c m_r m_l k_f p_{n-j} - \left(A_c m_r m_l k_f + n k_r^{(n)}\right) p_n + (n+1)\, k_r^{n+1} p_{n+1} \quad (2)$$

where p_n is the probability of having n bonds at time t and $k_r^{(n)}$ is the reverse rate for the dissociation of the nth bond. In a Couette flow, such as the one being modeled in the present study, mechanical forces are applied to the formed doublets, and the forced dissociation of existing bonds follows the Bell model: $k_r^{(n)} = k_r^0$ (4). Here, k_r^0 is the zero-force reverse rate, a is the interaction range, $F(t)$ is the force shared among n bonds [a periodic function of time for doublet rotation in shear flow (24,34)], k_B is the Boltzmann constant, and T is the absolute temperature. It is important to note that shear force has little impact on doublet dissociation, and only normal force is taken into consideration for the forced dissociation of formed bonds (24).

In our previous model (24), the effective forward rate $A_c m_r m_l k_f$ was assumed to be constant over simulation for all receptor-ligand pairs cross-linking the doublets. However, several reports from the cone-plate shear experiments indicated that the avidity decreased after cytokine stimulation even though the expressions of β_2-integrin on PMNs and ICAM-1 on WM9 cells were upregulated (29,43). To account for this decrease, an exponential-decay model for the effective forward rate was proposed in the present simulation:

$$(A_c m_r m_l k_f)(t) = (A_c m_r m_l k_f)^0 e^{-\alpha t} \quad (3)$$

where $(A_c m_r m_l k_f)(t)$ and $(A_c m_r m_l k_f)^0$ are the effective forward rates, respectively, at time t and immediately after stimulation ($t = 0$). The decay factor α, which was previously introduced by Neelamegham et al. (29) in a deterministic model for homotypic neutrophil aggregations, describes the time-dependent changes in cell adhesiveness.

Numerical calculation strategies

Shear-induced formation and breakage of PMN and WM9 heterotypic doublets were predicted by using the above model. Since the most aggregates were found to be PMN-WM9 heterotypic doublets (>90%) (Fig. 1*A*), it is reasonable to neglect the effects of multiplets (>2) when predicting the aggregation kinetics. In a Couette flow to be considered here, the formation of new doublets mediated by one bond and the evolution of formed bonds in existing doublets were coupled to determine the percentage of doublets at time *t*. To track this percentage, the initial value of aggregation percentage at $t = 0$ was assumed to be zero, the newly formed doublets were added into a doublet pool, and the multiple singlet dissociated from existing doublets was pooled into a singlet subgroup at an arbitrary time t ($t > 0$).

In the current numerical calculations, two strategies were taken to fit the data with the model. One was global fitting, in which different data sets at different shear rates and medium viscosities were pooled together and a single set of four parameters [k_r^0, a, $(A_c m_r m_l k_f)^0$, and α] was used (cf. Table 2). The other was individual fitting, in which an individual set of three parameters [k_r^0, $(A_c m_r m_l k_f)^0$, and α] was used at each shear rate and medium viscosity, together with an estimated interaction range, a, from global fitting (cf. Table 2). In individual fitting, it is hard to adjust independently the kinetic parameters (k_r^0 and a) from the Bell model. This is different from global fitting, which lumps the data with at least two shear rates and can predict two parameters respectively. Thus, global fitting was not performed for the three cases of aggregation between fMLP-stimulated PMNs and TNF-α-stimulated WM9 cells, since it is unknown whether stimulating WM9 cells with various TNF-α concentrations induces conformational changes in ICAM-1, which could vary the 2D kinetics of β_2-integrin-ICAM-1 interactions.

Data analysis

The analytical solution to Eq. 2 was no longer possible, since the force acting on the rotating doublets varied continuously with time. A modified Levenberg-Marquart method and a Runge-Kutta numerical scheme were used to fit the probabilistic model to the measured percentages of heterotypic aggregation. The resulting probability of forming a nonzero number of bonds, $1\text{-}p_0(t)$, was compared with the aggregation percentage at time t, where $p_0(t)$ represents the fraction of singlet.

The best fit of the above numerical calculation was obtained by adjusting a set of kinetic parameters [k_r^0, a, $(A_c m_r m_l k_f)^0$, and α] (four-parameter prediction for global fitting) or [k_r^0, $(A_c m_r m_l k_f)^0$, and α] (three-parameter prediction for individual fitting) that minimized the error (χ^2) between the data and the predictions (31). The χ^2 statistic, or weighted sum of square of errors, was defined by

$$\chi^2 = \sum_{i=1}^{N} [y_i - y(x_i)]^2 / \sigma_i^2$$

where y_i, $y(x_i)$, and σ_i are the measurement, prediction, and standard deviation at x_i, respectively, and N is the number of data points. Since the standard deviations of measured aggregation percentages were significantly different with different shear durations for an individual aggregation percentage and the smallest deviation contributes to the largest χ^2 statistic, the average standard deviation

$$\bar{\sigma}\left(=\sum_{i=1}^{N}\sigma_i/N\right)$$

was used for all data points in that case to normalize the fluctuations of each data point. The reduced χ^2 statistic, χ_ν^{22}, where ν is the number of degrees of freedom (= $N - N_f$, where N_f is the number of fitting parameters), can be used to measure both the appropriateness of the proposed model and the quality of the data. The statistical significance of the difference between the 2D kinetic rates and the binding affinities of the β_2-integrin-ICAM-1 pairs in different shear rates and medium viscosities with different chemotactic simulations was assessed using Student's *t*-test.

RESULTS

Aggregations of fMLP-stimulated PMNs and WM9 cells in a shear flow

During their passage through the circulatory system, tumor cells undergo extensive interactions with various host cells including PMNs, which are regulated by the hydrodynamic shear flow. By using a cone-plate viscometer, the heterotypic aggregation of WM9 cells and PMNs was characterized over a range of shear conditions and media viscosities. Application of shear resulted in formation of heterotypic aggregation consisting of a melanoma cell bound to a PMN, which could be detected by the two-color flow cytometry (Fig. 1*A*). Results indicated that PMNs or WM9 cells alone fell into specific fluorescence channels in shear flow, which was different than the heterotypic aggregation between PMNs and WM9 cells. The population of WM9 cells was resolved into singlet and aggregates composed of a single WM9 cell bound to one, two, or more than two PMNs. The concentrations of these aggregates were represented by [WM9], [TP_1], [TP_2], and [TP_{3+}], respectively. Most aggregates were found to be PMN-WM9 heterotypic doublets (TP_1; >90%). Results showed that shear flow resulted in formations of heterotypic aggregation, which is regulated by the shear duration and hydrodynamic forces. As shown in Fig. 1*B*, the percentage of WM9 tumor cells in aggregation reached a maximum fraction at t = 60 s and then started to descend, possibly because of the disaggregation of the heterotypic aggregates after longer durations (100 −300 s) of shear exposure for all the shear rates tested (62.5− 800 s^{-1}) at a given viscosity (η = 1.0 cP). In addition, more WM9 cells were found to form aggregations with PMNs at a low shear rate, 62.5 s^{-1}, whereas high shear rates (400 − 800 s^{-1}) significantly decreased the aggregations between WM9 cells and PMNs (Fig. 1*B*).

Shear rates affect aggregation of PMNs and WM9 cells

Our recent studies using a flow chamber assay have reported that PMN-facilitated melanoma adhesion to the EC could be a two-step process, which is shear-rate dependent (18). However, it is not clear how aggregations between PMNs and melanoma cells are affected by the shear rates. Current experimental results indicated that the aggregation percentage remained nearly the same when the shear stress varied from 0.625, 1.25, to 2 dyn/cm^2 at a fixed shear rate G = 62.5 s^{-1} (Fig. 2*A*) and from 2, 4, to 6.4 dyn/cm^2 at G = 200 s^{-1} (Fig. 2*B*). In contrast, the aggregation percentage inversely increased when G was reduced from 200 to 62.5 s^{-1} under a fixed shear stress of 2 dyn/cm^2 (Fig. 2*C*) and from 400 to 200 s^{-1} under 4 dyn/cm^2 (Fig. 2*D*),

suggesting that the shear-induced aggregation of fMLP-stimulated PMNs and WM9 cells is shear-rate dependent.

PMN-WM9 aggregations depend on specific β_2-integrin-ICAM-1 interactions

Previous studies have shown that LFA-1 and Mac-1 on PMN incorporated to capture melanoma cells by binding to ICAM-1 on melanoma cells, which brought the melanoma cells close to the EC (18). To explore whether there are other possible receptor-ligand bindings between PMNs and melanoma cells that may mediate heterotypic aggregations, flow cytometry was used to detect adhesion molecule expressions on WM9 cells. Results indicated that Mac-1, LFA-1, sLe^x, sLe^a, E-selectin, and P-selectin were not found on WM9 cells, whereas significant ICAM-1 expression was detected (Table 1), which implied that heterotypic aggregation of PMNs and melanoma cells is mostly mediated through the interactions of β_2-integrin and ICAM-1.

To test whether β_2-integrin-ICAM-1 interactions affect the heterotypic aggregation, PMNs and WM9 cells were treated with fMLP and TNF-α, respectively, and the PMN-WM9 aggregations were measured. Results indicated that after fMLP stimulation, the Mac-1 expression on PMNs increased significantly (Fig. 3*A*). ICAM-1 expressions on TNF-α-stimulated WM9 cells were also upregulated at TNF-α concentrations of 10 and 100 U/ml, whereas there were no differences in ICAM-1 expressions for unstimulated and stimulated WM9 cells at low concentration of 1 U/ml (Fig. 3*A*). In addition, time-dependent expressions of LFA-1 and Mac-1 on PMNs as well as of ICAM-1 on WM9 cells were also investigated under a shear condition. Results showed that there was no difference in LFA-1 expression between nonstimulated and fMLP-stimulated PMNs even though expression of LFA-1 increased over time for both nonstimulated and fMLP-stimulated cases (Fig. 3*B*). In contrast, Mac-1 expression on fMLP-stimulated PMNs was significantly higher than that on nonstimulated PMNs. Mac-1 expression on fMLP-stimulated PMNs increased over time, whereas its expression on nonstimulated PMNs did not change very much (Fig. 3*C*). The ICAM-1 expression on WM9 cells increased significantly after TNF-α stimulation. However, it did not change in the entire shear duration (Fig. 3*D*).

No matter if PMNs were fMLP-stimulated, shear-induced aggregation of PMNs and WM9 cells exhibited a transition phase in which the aggregation fraction increased with shear duration t up to 60 s, reaching an equilibrium phase with a plateau beyond $t > 120$ s (Fig. 4*A*). But the aggregation percentage was significantly lowered for unstimulated PMNs than fMLP-stimulated PMNs ($t < 120$ s) at the same shear rate 200 s^{-1} (Fig. 4*A*). In addition, stimulation of WM9 cells using TNF-α (e.g., at 10 and 100 U/ml) significantly increased the WM9-PMN heterotypic aggregations compared with control cases without TNF-α stimulation (Fig. 4*B*). Functional blocking of β_2-integrin on PMNs or ICAM-1 on WM9 cells almost demolished the heterotypic aggregation of PMNs and WM9 cells (Fig. 4*C*), suggesting that the specific binding between β_2-integrin on PMNs and ICAM-1 on WM9 cells is critical for the formation of PMN-WM9 aggregations.

2D kinetics of β_2-integrin and ICAM-1 binding

To quantify the 2D kinetics of shear-induced aggregation and disaggregation of PMN-WM9 interactions, a previously developed probabilistic model (Eqs. 2 and 3), together with a two-body collision theory, was used to predict the time dependence of aggregation percentages. As shown in Fig. 5, the predictions (lines), obtained from the individual fitting and plotted using the best-fitted parameters, were in an excellent agreement with the data (points). The predictions from the global fitting (data not shown) were also in a good agreement with those from the individual fitting, suggesting that the model prediction is reliable. The qualities of best-fitting (χ^2) are listed in Table 2, with best fit depending mainly on the standard deviation

of the measured data. The highest χ^2 value (115.14) was due to less best-fitting to those two cases at a high shear rate (200 s^{-1}) with both medium viscosities of $\eta = 2.0$ and 3.2 cP (data not shown), which is still reasonable when four parameters were used to best-fit total 45 data points in global fitting.

Kinetic parameters and decay factors obtained by fitting the model to the data of PMN-WM9 aggregation kinetics are summarized in Table 2. The mean and standard error of the kinetic parameters k_r^0 and $(A_c m_r m_l k_f)^0$ and of the decay factor α were estimated by averaging the parameters calculated by best-fitting the data for each individual case. Zero-force reverse rate, k_r^0, for fMLP-stimulated PMNs was similar to that for unstimulated PMNs (0.57 ± 0.08 and 0.33 ± 0.10 s^{-1}, respectively; $P > 0.1$). Effective forward rate, $(A_c m_r m_l k_f)^0$, although being 2.1-fold higher for fMLP-stimulated PMNs, was not significantly different from that for unstimulated PMNs (3.39 ± 0.56 and 1.60 ± 0.46 s^{-1}, respectively; $P > 0.1$) when they respectively interacted with unstimulated WM9 cells. Decay factor α appeared to be insensitive to stimulation for PMNs [(1.29 ± 0.22) and (0.61 ± 0.16) $\times 10^{-3}$ s^{-1} for fMLP-stimulated and -unstimulated PMNs, respectively; $P > 0.1$]. These kinetic parameters and decay factor for fMLP-stimulated PMNs were similar to those when fMLP-stimulated PMNs interacted with TNF-α-stimulated WM9 cells at 1 U/ml [k_r^0, $(A_c m_r m_l k_f)^0 = 3.52$, and $\alpha = 1.84 \times 10^{-3}$ s^{-1}], suggesting that stimulating WM9 cells with low TNF-α concentration has no significant impact on 2D kinetics of β_2-integrin-ICAM-1 interactions. At 10 and 100 U/ml TNF-α concentrations, however, zero-force reverse rates (0.93 and 1.97 s^{-1}, respectively) were 1.6- and 3.3-fold higher, and effective forward rates (6.16 and 14.52 s^{-1}, respectively) were 1.8- and 4.1-fold higher than those at 1 U/ml, whereas the decay factors (0.43 and 0.14 s^{-1}, respectively) were much smaller than that at 1 U/ml. Moreover, the mean values of two kinetic parameters and decay factor obtained from individual fitting were in excellent agreements with those obtained from global fitting (Table 2). The interaction range, *a*, obtained from global fitting (0.41 and 0.53 $\times 10^{-10}$ m for fMLP-stimulated and -unstimulated PMNs, respectively) was similar to that previously obtained for $\alpha_4\beta_7$-integrin (0.41×10^{-10} m) (8). Blockage of β_2-integrin and ICAM-1, respectively, reduced zero-force reverse rate and effective binding affinity significantly, but not interaction range (Table 2), imparting the confidence that nonspecific interactions between other surface adhesive molecular pairs induced a low-level baseline PMN-WM9 aggregation. Taken together, these results of 2D kinetics for β_2-integrin-ICAM-1 binding were consistent with experimental observations in aggregation kinetics of PMN-WM9 interactions, providing quantitative understanding of melanoma cell aggregations to PMNs under shear conditions, as well as further validation to the model.

Numerical analysis on kinetics parameters

Further analyses of the kinetic parameters and decay factor were performed with the numerical calculations for aggregation of fMLP-stimulated PMNs and unstimulated WM9 cells at $G = 100$ s^{-1} and $\eta = 1.0$ cP. To isolate the dependence of the aggregation kinetics on individual parameters, one parameter was varied in each calculation. As shown in Fig. 6, the maximum aggregation percentage shifted upward to the right when the zero-force reverse rate was lowered, suggesting that the lower reverse rate enhances the total aggregation and prolonged the ascending phase (Fig. 6*A*). In contrast, it shifted downward to the left when the effective forward rate at $t = 0$ was lowered, implying that the lower forward rate decreases the total aggregation and shortened the ascending phase (Fig. 6*B*). The aggregation percentage shifted upward to the right when the interaction range (Fig. 6*C*) or the decay factor was decreased (Fig. 6*D*). These results show that the kinetic parameters k_r^0, *a*, and $(A_c m_r m_l k_f)^0$ and decay factor α specifically regulate the PMN-WM9 aggregation kinetics.

DISCUSSION

Tumor metastasis consists of a complex cascade of adhesive interactions between tumor cells and host cells including PMNs (20). PMNs actively participate in the inflammatory response through adhesion to the activated EC, which is mediated by sialylated molecules and β_2-integrins expressed on PMNs. Not all melanoma cells express β_2-integrins or sialylated molecules at levels effectively to adhere to the EC by themselves under shear conditions (49). However, malignant melanoma cells constitutively express a high level of ICAM-1, the ligand for β_2-integrins. Therefore, melanoma cells could arrest on the EC via binding to PMNs that may bring tumor cells close to the EC and thus facilitate melanoma cells extravasation through the EC within the microcirculation (18). Little is known or understood, however, of the binding kinetics between melanoma cells and PMNs within the blood flow. The goal of the present study was to quantify the aggregation kinetics of WM9 melanoma cells and PMNs in a shear flow and to correlate them with the kinetics underlying β_2-integrins-ICAM-1 bindings.

PMN-facilitated melanoma adhesion to and subsequent migration through the EC appears to be a “two-step” process that involves initial PMN tethering on the EC and subsequently melanoma cells being captured by tethered PMNs (18). This process could be a result of regulation of IL-8 expression in melanoma-stimulated PMN inflammatory response and activation (30). PMN tethering has been found to be both shear-rate and shear-stress dependent, although melanoma cell adhesion to the EC via tethered PMNs has been shown to be shear-rate dependent only (18,37). However, little is known regarding the mechanisms involved. In the present study, using a cone-plate viscometer to generate a uniform shear field, aggregations between melanoma cells and PMNs have been characterized and quantified to investigate the mechanism of the shear-rate-dependent melanoma adhesion to the EC mediated by PMNs. Our results have indicated that hydrodynamic shear regulates PMN-WM9 heterotypic aggregation that is dependent on shear rates rather than shear stresses. The heterotypic aggregation appears to peak after ~60 s under the shear and starts to decrease afterward. Early stage of fluid shear may increase PMN-WM9 cell interactions modulated by cell-cell collisions; however, the accumulated tensile forces may overweigh the strength of cell-cell adhesive bonds and break up the aggregations after a longer exposure to the shear. Relative velocities of cells in a fluid field are determined by the shear rate that modulates the collision frequency and contact time between cells. A lower shear rate increases the time that cells are in contact, thus having higher probability of formation for WM9-PMN aggregations. On the other hand, shear stress dictates the forces applied to cells individually and the intermolecular bonds between the cells. The shear-rate dependence of melanoma cells and PMNs aggregation found from this aggregation study elucidates a possible mechanism that explains why melanoma cell adhesion to the EC facilitated by PMNs under flow conditions is influenced by the hydrodynamic shear rates.

Similar findings in shear-rate-dependent bond formation has been reported when individual PSGL-1-expressing PMNs roll over and tether to a P-selectin-immobilized substrate (5), suggesting that P-selectin and PSGL-1 bond formation could also be a function of shear rate, hence the kinetics of receptor and ligand association. In contrast, the kinetics of bond dissociation is a function of shear stress, therefore the force on the bonds (5). Other studies have shown that LFA-1, Mac-1, and L-selectin on PMNs are requisite for the heterotypic aggregation with colon carcinoma-expressing ICAM-1, sialylated molecules, and CD44 (11, 15,16). Expression of variant isoforms of CD44 on melanoma cells also has been reported (32), which may potentially mediate interactions of PMNs and melanoma cells through L-selectin on PMNs and CD44 on melanoma cells. In the present study, however, we have shown that blocking either ICAM-1 on WM9 cells or β_2-integrins on PMNs almost abolished heterotypic WM9-PMN aggregation, indicating ICAM-1 bindings to β_2-integrins may play more influential roles than other receptors in mediating the WM9-PMN aggregation in a shear

flow. fMLP was used to regulate the β_2-integrin expressions on PMNs, which allowed us to investigate the effects of PMN activation on heterotypic aggregation of PMN and melanoma cells. Results have clearly indicated that the existence of inflammatory stimulus could boost the PMN-melanoma cell aggregation under shear conditions. We have found LFA-1 expression on PMNs remains to be about the same after fMLP stimulation, which is comparable to LFA-1 expression on resting PMNs (3). In contrast, fMLP stimulation results in an increase in Mac-1 expression that can reach a plateau within 2−4 min (3,14). An increased expression in Mac-1 may contribute to a higher extent of melanoma cells binding to fMLP-stimulated PMNs than that to unstimulated PMNs in response to shear exposure in short times (e.g., up to 120 s). However, after a long exposure to the shear, there are no significant differences in WM9-PMN aggregation between fMLP-stimulated and unstimulated cases. The possible explanation is that the increase in aggregation is rather transient because previous studies have also shown increased CD11b/CD18 avidity could be reversed over minutes unless increasing stimulus would be further applied (14,22). In addition, a recent study has reported that CD18 expression could be downregulated on long exposure to fluid shear (10). Therefore, the differences in CD18 expression from fMLP-stimulated and unstimulated PMNs may diminish after a longer exposure to the shear.

There is now evidence that inflammatory cytokines and chemokines, which can be produced by the tumor cells and/or tumor-associated leucocytes and platelets, may contribute directly to malignant progression (7,21). For example, previous studies have shown that interactions of PMN and melanoma cells can induce increased secretion of inflammatory cytokine IL-8 from a tumor microenvironment (30) and IL-8 has been shown to upregulate the expression of β_2-integrins on PMNs (9,19). This may further enhance the binding between ICAM-1 on melanoma cells and β_2-integrins on PMN and thus facilitate melanoma cell adhesion to the EC via PMNs during the extravasation process in metastasis.

A probabilistic kinetic model together with Smoluchowski's two-body collision theory has been applied to describe the formation and breakage of doublets of PMNs and melanoma cells mediated by β_2-integrin-ICAM-1 binding. Not only has this probabilistic model been extensively used to predict 2D kinetics of receptor-ligand bindings, but it is also able to estimate intrinsic kinetic rates and binding affinities of the interacting molecules (6,13,47). For example, our results indicate that zero-force reverse rate agrees well with those published previously (8,23,50). Although two types of β_2-integrin receptors are involved in PMN-WM9 aggregation, and a concurrent binding model of multiple molecular species in cell adhesion has been developed by Zhu and Williams (51), it appears to be rather difficult to extract two set of the kinetics parameters from the current data sets (6 parameters to fit 5 data points per curve in individual fitting). Kinetic parameters appearing in the current model are physiologically correlated to the aggregation dynamics of WM9-PMN interactions. Forward or reverse rate determines, respectively, how fast a β_2-integrin-ICAM-1 bond forms or dissociates (also how fast a WM9-PMN doublet aggregates or disaggregates). The effective binding affinity, $(A_c m_r m_l K_a)^0 \left[= (A_c m_r, m_l, k_f)^0 / k_r^0 \right]$, governs how likely the bond remains bound in an equilibrium state. With a higher TNF-α concentration (10 or 100 U/ml), for example, a higher reverse rate of β_2-integrin-ICAM-1 interaction suggests that the aggregations between TNF-α-stimulated WM9 cells and fMLP-stimulated PMNs are not as stable as that for unstimulated WM9 cells with either fMLP-stimulated or -unstimulated PMNs, whereas a higher forward rate implies that stimulated WM9 cells are more likely to form aggregations than that for unstimulated WM9 cells with PMNs (stimulated or unstimulated). A similar effective binding affinity (4.79~7.37) shows that TNF-α stimulation would not affect the equilibrium binding between WM9 and PMN cells. The interaction range, *a* (i.e., an estimate of mechanical bond strength), is not sensitive to chemotactic regulations, as reported in the literature for selectin-ligand and

other adhesion molecules (8). The present findings provide a clue for screening the potential therapeutic targets in preventing PMN-tumor cell adhesions and subsequent metastasis.

We have also proposed an exponentially decay- and time-dependent effective forward rate $A_c m_r m_l k_f$ (Eq. 3) in the present study to predict the biphasic time-dependent course of PMN-WM9 aggregations. Similar biphasic time dependence was previously found in PMN homotypic aggregation mediated by the transition from L-selectin- to β_2-integrin-dependent adhesion (43), and an exponentially decay in time of adhesion efficiency was also proposed (29). Estimated values of decay factor α for PMN-WM9 interaction in the current study ($0.14\sim2.0 \times 10^{-3}$ s^{-1}) are similar to those for aggregations between PMNs and ICAM-1-transfected cells ($3\sim11 \times 10^{-3}$ s^{-1}) (28), but lower than those for PMN homotypic aggregations ($13\sim31 \times 10^{-3}$ s^{-1}) (29). Decay factor α is assumed to be governed by the contact area (A_c), receptor., and/or ligand expression (m_r, m_l), and even the molecular conformation changes. The contact area between two adjacent fMLP-stimulated PMNs at 180 s was reduced by ~70% compared with that at 30 s (29). β_2-Integrin could move to the uropod after PMNs being stimulated by fMLP, which reduces the number of interacting molecules within the contact area (14). Although the expression of β_2-integrin on PMNs is upregulated, the rapid activation of LFA-1 is transient and reversible within ~30 s, whereas the active conformation of Mac-1 is stable beyond 10 min during shear (36). The effective forward rates $(A_c k_f)^0$ at $t = 0$ from $(A_c m_r m_l k_f)^0$ for the PMN-WM9 aggregations were found to be 0.014 (between fMLP-stimulated PMNs and unstimulated WM9 cells), 0.010 (between unstimulated PMNs and unstimulated WM9 cells), 0.013, 0.013, and 0.024 (between fMLP-stimulated PMNs and stimulated WM9 cells by TNF-α at 1, 10, and 100 U/ml, respectively), indicating that the increasing effective forward rate is mostly caused by the increasing expression of adhesion molecules.

Finally, the time course of aggregation percentage between PMNs and WM9 melanoma cells exhibits a biphasic transition and shear-rate dependence. A modified probabilistic kinetic model presented in the current study reproduces the data well and enables us to quantify the kinetic rates and affinities of interacting β_2-integrin and ICAM-1 bindings between PMNs and tumor cells. These findings provide a rationale and mechanistic basis for understanding leukocyte-tumor cell interactions mediated by specific receptor-ligand interactions under flow conditions, which provides insights into potential targets in inhibiting PMN-mediated melanoma extravasation and subsequent metastasis development.

ACKNOWLEDGMENTS

We thank Dr. M. Herlyn from Wistar Institute, Philadelphia, PA, for providing WM9 melanoma cells. The authors also acknowledge the Penn State General Clinical Research Center (GCRC) staff for assistance with blood sample collection and for providing nursing care.

GRANTS

This work was supported in part by National Institutes of Health (NIH) Grants CA-97306 and CA-125707; National Science Foundation (NSF) Grant CBET-0729091; and the Penn State Biomaterials and Bionanotechnology Summer Institute, funded by NSF Grants EEC-0234026 and EEC-0609053 (to C. Dong), and by the National Key Basic Research Foundation of China Grant 2006CB91303, National Science Foundation of China Grants 30730032, 10332060, and 30225027, and Chinese Academy of Sciences Grant 2005-1-16 (to M. Long). The Penn State GCRC is funded in part by NIH Grants M01-RR-010732 and C06-RR-016499.

REFERENCES

1. Adler PM. Interaction of unequal spheres.: I. Hydrodynamic interaction: Colloidal forces. J Colloid Interface Sci 1981;84:461–473.
2. Alon R, Kassner PD, Carr MW, Finger EB, Hemler ME, Springer TA. The integrin Vla-4 supports tethering and rolling in flow on VCAM-1. J Cell Biol 1995;128:1243–1253. [PubMed: 7534768]

3. Bateman J, Parida SK, Nash GB. Neutrophil integrin assay for clinical studies. Cell Biochem Funct 1993;11:87–91. [PubMed: 8100744]
4. Bell GI. Models for the specific adhesion of cells to cells. Science 1978;200:618–627. [PubMed: 347575]
5. Chen SQ, Springer TA. Selectin receptor-ligand bonds: Formation limited by shear rate and dissociation governed by the Bell model. Proc Natl Acad Sci USA 2001;98:950–955. [PubMed: 11158576]
6. Chesla SE, Selvaraj P, Zhu C. Measuring two-dimensional receptor-ligand binding kinetics by micropipette. Biophys J 1998;75:1553–1572. [PubMed: 9726957]
7. Coussens LM, Werb Z. Inflammation and cancer. Nature 2002;420:860–867. [PubMed: 12490959]
8. De Chateau M, Chen SQ, Salas A, Springer TA. Kinetic and mechanical basis of rolling through an integrin and novel Ca^{2+}-dependent rolling and Mg^{2+}-dependent firm adhesion modalities for the alpha 4 beta 7-MAdCAM-1 interaction. Biochemistry 2001;40:13972–13979. [PubMed: 11705388]
9. Diamond MS, Springer TA. The dynamic regulation of integrin adhesiveness. Curr Biol 1994;4:506–517. [PubMed: 7922371]
10. Fukuda S, Schmid-Schonbein GW. Regulation of CD18 expression on neutrophils in response to fluid shear stress. Proc Natl Acad Sci USA 2003;100:13152–13157. [PubMed: 14595007]
11. Hanley WD, Napier SL, Burdick MM, Schnaar RL, Sackstein R, Konstantopoulos K. Variant isoforms of CD44 are P- and L-selectin ligands on colon carcinoma cells. FASEB J 2005;19:337–339. [PubMed: 16352650]
12. Hentzen ER, Neelamegham S, Kansas GS, Benanti JA, McIntire LV, Smith CW, Simon SI. Sequential binding of CD11a/CD18 and CD11b/CD18 defines neutrophil capture and stable adhesion to intercellular adhesion molecule-1. Blood 2000;95:911–920. [PubMed: 10648403]
13. Huang J, Chen J, Chesla SE, Yago T, Mehta P, Mcever RP, Zhu C, Long M. Quantifying the effects of molecular orientation and length on two-dimensional receptor-ligand binding kinetics. J Biol Chem 2004;279:44915–44923. [PubMed: 15299021]
14. Hughes BJ, Hollers JC, Crocketttorabi E, Smith CW. Recruitment of Cd11B/Cd18 to the neutrophil surface and adherence-dependent cell locomotion. J Clin Invest 1992;90:1687–1696. [PubMed: 1358917]
15. Jadhav S, Bochner BS, Konstantopoulos K. Hydrodynamic shear regulates the kinetics and receptor specificity of polymorphonuclear leukocyte-colon carcinoma cell adhesive interactions. J Immunol 2001;167:5986–5993. [PubMed: 11698478]
16. Jadhav S, Konstantopoulos K. Fluid shear- and time-dependent modulation of molecular interactions between PMNs and colon carcinomas. Am J Physiol Cell Physiol 2002;283:C1133–C1143. [PubMed: 12225977]
17. Kwong D, Tees DFJ, Goldsmith HL. Kinetics and locus of failure of receptor-ligand-mediated adhesion between latex spheres. 2. Protein-protein bond. Biophys J 1996;71:1115–1122. [PubMed: 8842248]
18. Liang S, Slattery MJ, Dong C. Shear stress and shear rate differentially affect the multi-step process of leukocyte-facilitated melanoma adhesion. Exp Cell Res 2005;310:282–292. [PubMed: 16154563]
19. Liang SL, Sharma A, Peng HH, Robertson G, Dong C. Targeting mutant (V600E) B-Raf in melanoma interrupts immunoediting of leukocyte functions and melanoma extravasation. Cancer Res 2007;67:5814–5820. [PubMed: 17575149]
20. Lichtenstein A. Stimulation of the respiratory burst of murine peritoneal inflammatory neutrophils by conjugation with tumor cells. Cancer Res 1987;47:2211–2217. [PubMed: 3032419]
21. Liotta LA, Kohn EC. The microenvironment of the tumour-host interface. Nature 2001;411:375–379. [PubMed: 11357145]
22. Lo SK, Detmers PA, Levin SM, Wright SD. Transient adhesion of neutrophils to endothelium. J Exp Med 1989;169:1779–1793. [PubMed: 2565948]
23. Lomakina EB, Waugh RE. Micromechanical tests of adhesion dynamics between neutrophils and immobilized ICAM-1. Biophys J 2004;86:1223–1233. [PubMed: 14747356]
24. Long M, Goldsmith HL, Tees DFJ, Zhu C. Probabilistic modeling of shear-induced formation and breakage of doublets cross-linked by receptor-ligand bonds. Biophys J 1999;76:1112–1128. [PubMed: 9916043]

25. Lum AFH, Green CE, Lee GR, Staunton DE, Simon SI. Dynamic regulation of LFA-1 activation and neutrophil arrest on intercellular adhesion molecule 1 (ICAM-1) in shear flow. J Biol Chem 2002;277:20660–20670. [PubMed: 11929876]
26. McDonough DB, McIntosh FA, Spanos C, Neelamegham S, Goldsmith HL, Simon SI. Cooperativity between selectins and beta(2)-integrins define neutrophil capture and stable adhesion in shear flow. Ann Biomed Eng 2004;32:1179–1192. [PubMed: 15493506]
27. Miele ME, Bennett CF, Miller BE, Welch DR. Enhanced metastatic ability of TNF-alpha-treated malignant melanoma cells is reduced by intercellular adhesion molecule-1 (ICAM-1, Cd54) antisense oligonucleotides. Exp Cell Res 1994;214:231–241. [PubMed: 7915992]
28. Neelamegham S, Taylor AD, Burns AR, Smith CW, Simon SI. Hydrodynamic shear shows distinct roles for LFA-1 and Mac-1 in neutrophil adhesion to intercellular adhesion molecule-1. Blood 1998;92:1626–1638. [PubMed: 9716590]
29. Neelamegham S, Taylor AD, Hellums JD, Dembo M, Smith CW, Simon SI. Modeling the reversible kinetics of neutrophil aggregation under hydrodynamic shear. Biophys J 1997;72:1527–1540. [PubMed: 9083659]
30. Peng HH, Liang S, Henderson AJ, Dong C. Regulation of interleukin-8 expression in melanoma-stimulated neutrophil inflammatory response. Exp Cell Res 2007;313:551–559. [PubMed: 17141217]
31. Press, WH.; Flannery, BP.; Teukolsky, SA.; Vetterling, WT. Numerical Recipes in Fortran 77: The Art of Scientific Computing. Cambridge Univ. Press; Cambridge, UK: 1992. p. 675-683.
32. Seiter S, Schadendorf D, Herrmann K, Schneider M, Rosel M, Arch R, Tilgen W, Zoller M. Expression of CD44 variant isoforms in malignant melanoma. Clin Cancer Res 1996;2:447–456. [PubMed: 9816190]
33. Seo SM, McIntire LV, Smith CW. Effects of IL-8, Gro-α, and LTB_4 on the adhesive kinetics of LFA-1 and Mac-1 on human neutrophils. Am J Physiol Cell Physiol 2001;281:C1568–C1578. [PubMed: 11600420]
34. Shankaran H, Neelamegham S. Hydrodynamic forces applied on inter-cellular bonds, soluble molecules, and cell-surface receptors. Biophys J 2004;86:576–588. [PubMed: 14695302]
35. Shevde LA, Welch DR. Metastasis suppressor pathways - an evolving paradigm. Cancer Lett 2003;198:1–20. [PubMed: 12893425]
36. Simon SI, Green CE. Molecular mechanics and dynamics of leukocyte recruitment during inflammation. Annu Rev Biomed Eng 2005;7:151–185. [PubMed: 16004569]
37. Slattery MJ, Liang S, Dong C. Distinct role of hydrodynamic shear in leukocyte-facilitated tumor cell extravasation. Am J Physiol Cell Physiol 2005;288:C831–C839. [PubMed: 15601752]
38. Smoluchowski MV. Versuch einer mathematischen Theorie der Koagulationskinetik kolloider Losungen. Z Phys Chem 1917;92:129–168.in German
39. Soengas MS, Lowe SW. Apoptosis and melanoma chemoresistance. Oncogene 2003;22:3138–3151. [PubMed: 12789290]
40. Springer TA. Traffic signals for lymphocyte recirculation and leukocyte emigration - the multistep paradigm. Cell 1994;76:301–314. [PubMed: 7507411]
41. Tandon P, Diamond SL. Hydrodynamic effects and receptor interactions of platelets and their aggregates in linear shear flow. Biophys J 1997;73:2819–2835. [PubMed: 9370476]
42. Tandon P, Diamond SL. Kinetics of beta(2)-integrin and L-selectin bonding during neutrophil aggregation in shear flow. Biophys J 1998;75:3163–3178. [PubMed: 9826637]
43. Taylor AD, Neelamegham S, Hellums JD, Smith CW, Simon SI. Molecular dynamics of the transition from L-selectin- to beta(2)-integrin-dependent neutrophil adhesion under defined hydrodynamic shear. Biophys J 1996;71:3488–3500. [PubMed: 8968618]
44. Tees DFJ, Coenen O, Goldsmith HL. Interaction forces between red-cells agglutinated by antibody. 4. Time and force dependence of break-up. Biophys J 1993;65:1318–1334. [PubMed: 8241411]
45. Tees DFJ, Goldsmith HL. Kinetics and locus of failure of receptor-ligand-mediated adhesion between latex spheres. 1. Protein-carbohydrate bond. Biophys J 1996;71:1102–1114. [PubMed: 8842247]
46. Turitto VT. Blood viscosity, mass transport, thrombogenesis. Prog Hemost Thromb 1982;6:139–177. [PubMed: 6762611]

47. Wu L, Xiao B, Jia X, Zhang Y, Lu S, Chen J, Long M. Impact of carrier stiffness and microtopology on two-dimensional kinetics of P-selectin and P-selectin glycoprotein ligand-1 (PSGL-1) interactions. J Biol Chem 2007;282:9846–9854. [PubMed: 17267403]

48. Wu QD, Wang JH, Condron C, Bouchier-Hayes D, Redmond HP. Human neutrophils facilitate tumor cell transendothelial migration. Am J Physiol Cell Physiol 2001;280:C814–C822. [PubMed: 11245598]

49. Zetter BR. Adhesion molecules in tumor-metastasis. Semin Cancer Biol 1993;4:219–229. [PubMed: 8400144]

50. Zhang F, Marcus WD, Goyal NH, Selvaraj P, Springer TA, Zhu C. Two-dimensional kinetics regulation of alpha(L)beta(2)-ICAM-1 interaction by conformational changes of the alpha(L)-inserted domain. J Biol Chem 2005;280:42207–42218. [PubMed: 16234238]

51. Zhu C, Williams TE. Modeling concurrent binding of multiple molecular species in cell adhesion. Biophys J 2000;79:1850–1857. [PubMed: 11023890]

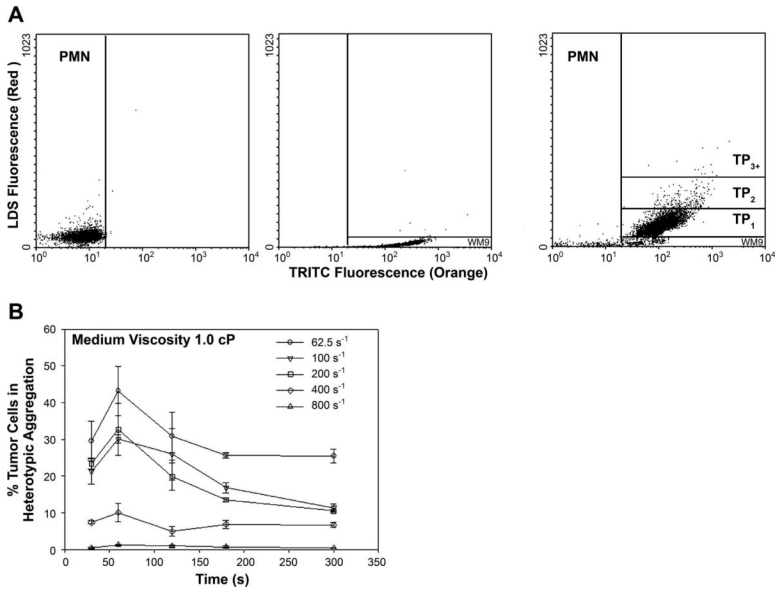

Fig. 1.

Flow cytometric detection of polymorphonuclear neutrophil (PMN)-WM9 heterotypic aggregation kinetics. PMNs (1×10^6 cells/ml) were labeled red (LDS-751), and WM9 cells (1×10^6 cells/ml) were stained orange [tetramethylrhodamine isothiocyanate (TRITC)] for 15 min at room temperature. Excess label was removed by washing and centrifugation, and cell populations were equilibrated in 37°C RPMI-1640 buffer containing 1% BSA, stimulated with 1 μM formyl-methionyl-leucyl-phenylalanine (fMLP), and sheared in a cone-plate viscometer at various shear rates. Samples were withdrawn at indicated time points, fixed with 2% cold formaldehyde, and analyzed on a flow cytometer. *A*: aggregate distribution 120 s after stimulation and application of shear. *Left*: PMNs only. *Middle*: WM9 melanoma cells only. *Right*: heterotypic aggregation of PMN-WM9. The population of WM9 cells was resolved into singlet and aggregates composed of a single WM9 cell bound to one, two, or more than two PMNs. The concentrations of these aggregates are represented by [WM9], [TP_1], [TP_2], and [TP_{3+}], respectively. The gating was based on the specific fluorescence channel in which each population fell. *B*: kinetics of aggregation of PMN-WM9 at different shear rates with medium viscosity at 1.0 cP. Values are means ± SE for $n \geq 3$.

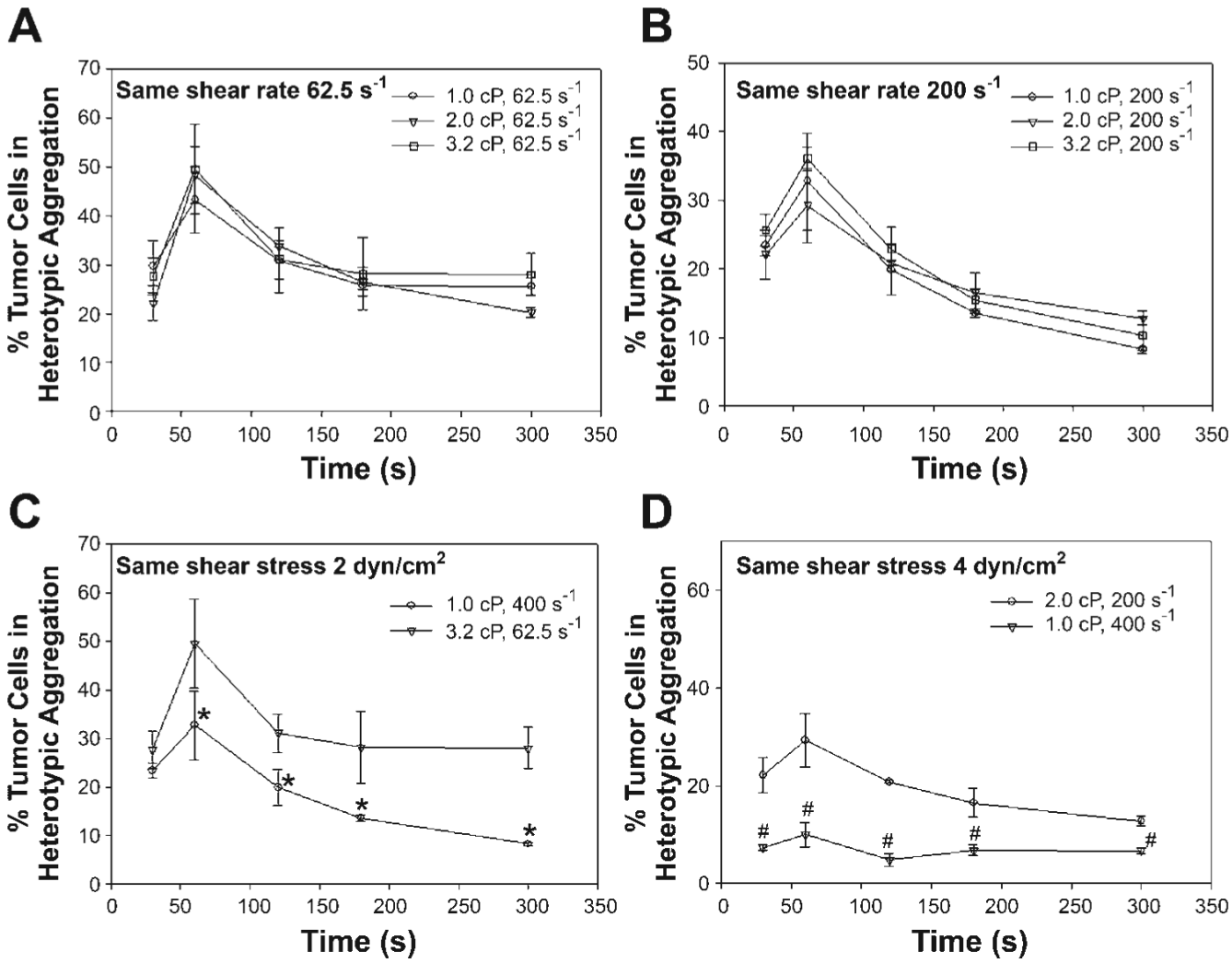

Fig. 2.

Effects of shear rate and shear stress on WM9 aggregation with fMLP-stimulated PMNs. Results show the percentage of melanoma cells in heterotypic aggregations: shear stress varied from 0.625, 1.25, to 2 dyn/cm^2 at a fixed shear rate 62.5 s^{-1} (*A*); shear stress varied from 2, 4, to 6.4 dyn/cm^2 at a fixed shear rate 200 s^{-1} (*B*); shear rate varied from 62.5 to 200 s^{-1} under a fixed shear stress 2 dyn/cm^2 (*C*); and shear rate varied from 200 to 400 s^{-1} under a fixed shear stress 4 dyn/cm^2 (*D*). *$P < 0.05$ with respect to 1.0 cP, 200 s^{-1} case; #$P < 0.05$ with respect to 2.0 cP, 200 s^{-1} case.

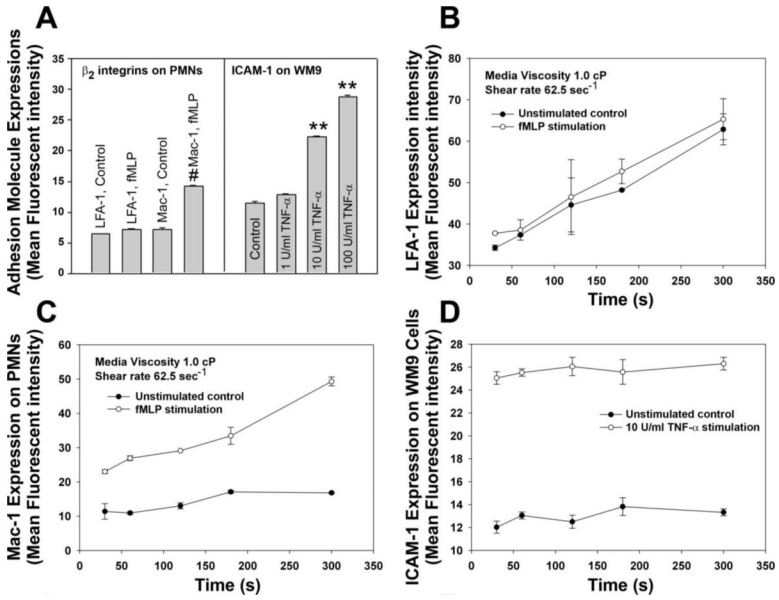

Fig. 3.

Expression of adhesion molecules. *A*: expressions of lymphocyte function-associated antigen-1 (LFA-1) and Mac-1 after PMNs were treated with 1 μM fMLP for 2 min and expression of ICAM-1 after WM9 cells were treated with various concentrations of TNF-α (1, 10, and 100 U/ml, respectively) for 24 h. #$P < 0.05$ and **$P < 0.05$ compared with respective controls. *B*: LFA-1 expression for various time points at 62.5 s^{-1} shear rate after PMNs were stimulated with 1 μM fMLP for 2 min. *C*: Mac-1 expression for various time points at 62.5 s^{-1} shear rate after PMNs were stimulated with 1 μM fMLP for 2 min. *D*: ICAM-1 expression for various time points at 62.5 s^{-1} shear rate after WM9 cells were stimulated with TNF-α for 24 h followed by resuspension in fresh media.

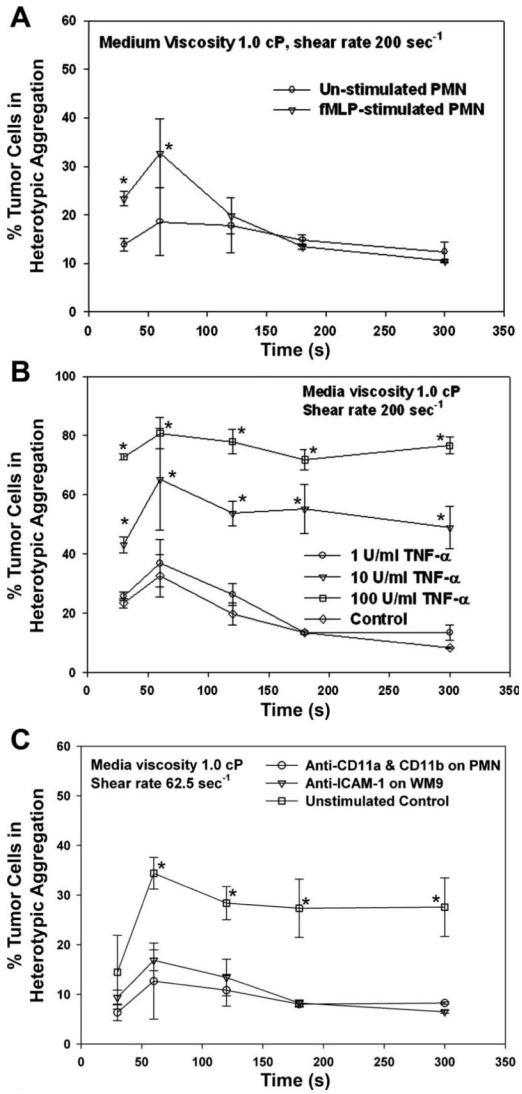

Fig. 4.

Effects of β_2-integrin and ICAM-1 binding on PMN-WM9 aggregations. *A*: percentage of WM9 aggregation with PMNs under the same shear condition, for both unstimulated and stimulated PMNs with 1 μM fMLP. **P* < 0.05 compared with unstimulated case. *B*: percentage of unstimulated or TNF-α-stimulated WM9 aggregation with fMLP-stimulated PMNs at shear rate 200 s^{-1}. The increase of tumor cell aggregation is related to the concentration of TNF-α used to stimulate WM9. **P* < 0.05 with respect to control cases without TNF-α stimulation on WM9 cells. *C*: blocking of either β_2-integrin on PMNs or ICAM-1 on WM9 significantly reduces PMN-WM9 aggregation compared with the control. **P* < 0.05 with respect to two antibody-blocking cases. Values are means ± SE for $n \geq 3$.

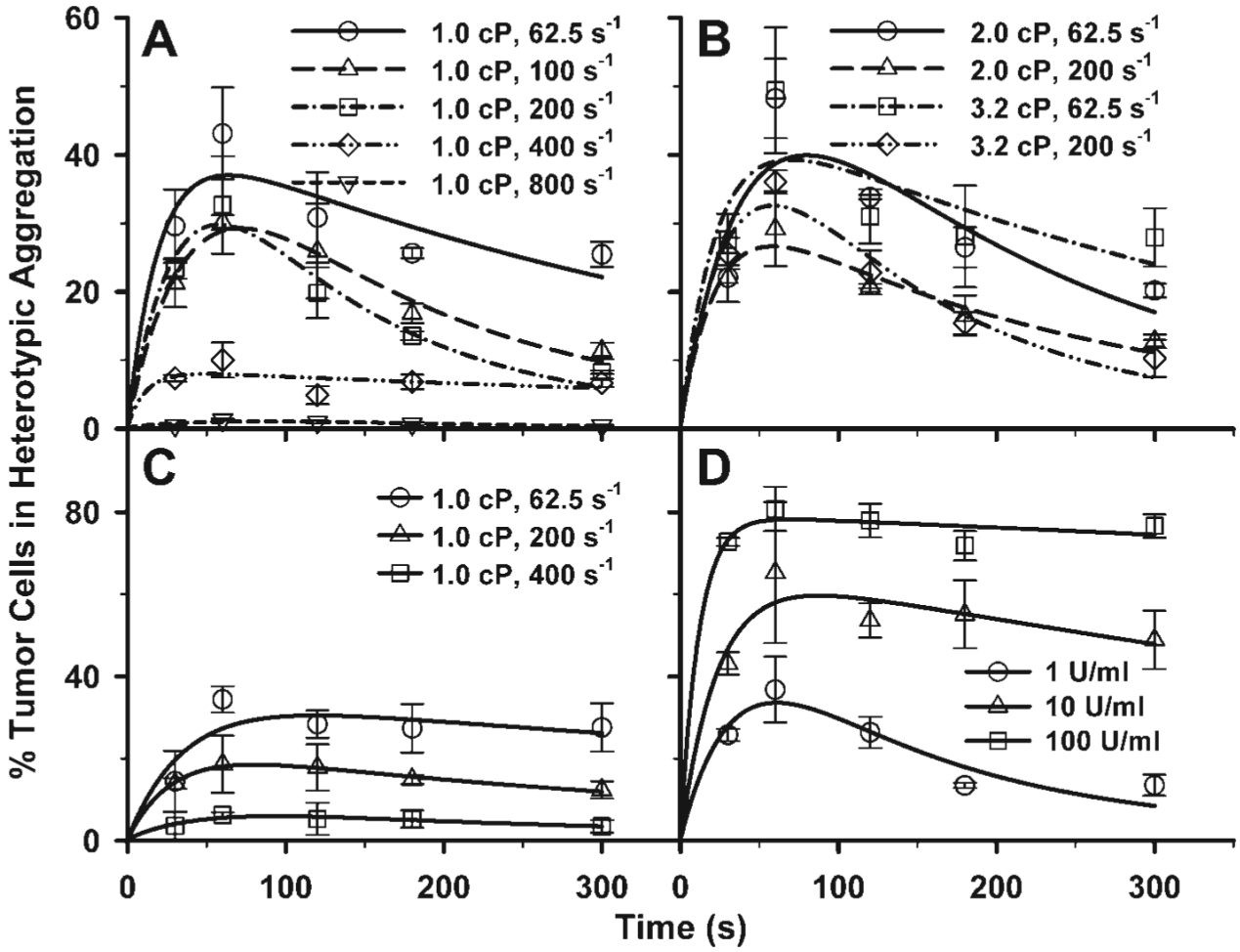

Fig. 5.

A probabilistic model predicting shear-induced PMN-WM9 aggregation fractions. *A*: fMLP-stimulated PMNs with unstimulated WM9 cells at shear rates 62.5, 100, 200, 400, and 800 s^{-1}, respectively, with medium viscosity of 1.0 cP. *B*: fMLP-stimulated PMNs with unstimulated WM9 cells at two different shear rates, 62.5 and 200 s^{-1}, with medium viscosity of 2.0 and 3.2 cP, respectively. *C*: unstimulated PMNs with unstimulated WM9 cells at shear rates 62.5, 200, and 400 s^{-1}, respectively, with medium viscosity of 1.0 cP. *D*: fMLP-stimulated PMNs with WM9 cells stimulated by TNF-α with three concentrations of 1, 10, and 100 U/ml, at shear rate 200 s^{-1} and medium viscosity 1.0 cP. Data are presented as means ± SE of aggregation percentages (points), which are in excellent agreements with the predictions (lines) using the probabilistic models. All predicted model parameters to fit the experimental data are presented in Table 2.

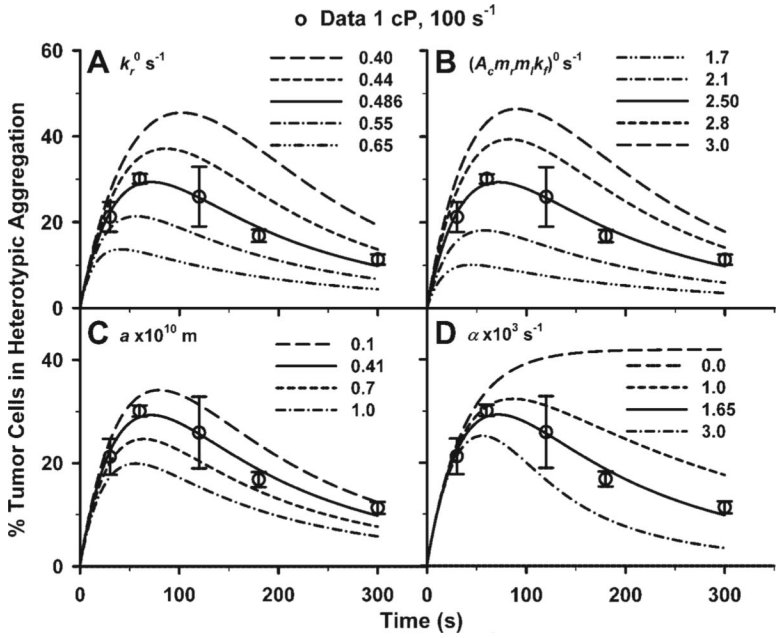

Fig. 6.

Parametric calculations with varied kinetic parameters and decay factors for unstimulated WM9 cell aggregation to fMLP-stimulated PMNs, at shear rate 100 s^{-1} and medium viscosity 1.0 cP for extended shear durations. Systematically varied zero-force reverse rate (k_r^0; *A*), effective forward rate [$(A_c m_r m_l k_f)^0$; *B*], interaction range (*a*; *C*), and decay factor (α; *D*) are shown. Also plotted are the measured data (points) and the fitted predictions (solid lines).

Table 1

Flow cytometric analysis of adhesion molecule expressions on WM9 cells

Receptor	Geometric Mean Fluorescence of WM9 Cells
Control IgG	0.67±0.03
(Control IgM)	(6.35±0.27)
(sLe^x)	(5.97±0.16)
(sLe^a)	(6.97±0.16)
LFA-1	0.8±0
Mac-1	0.60±0.05
ICAM-1	24.4±0.6
E-selectin	0.8±0.1
P-selectin	0.7±0.1

Values are geometric mean fluorescence intensities ± SE of three experiments using different batches of cells each time. The parentheses indicate that the antibody used to test the expressions of adhesive molecules is IgM antibody. LFA-1, lymphocyte function-associated antigen-1.

Table 2

Summary of kinetic parameters and decay factor of β_2-integrin and ICAM-1 bindings between PMNs and WM9 melanoma cells

Data Set	k_r^0, s^{-1}	$a \times 10^{10}$, m	$(A_c m_r m_l k_f)^0$, s^{-1}	$\alpha \times 10^3$, s^{-1}	χ^2
fMLP-stimulated PMNs with unstimulated WM9 cells (9 cases)					
Global fitting	0.62	0.41*	3.28	1.10	115.14
Individual fitting	0.57±0.08	0.41†	3.39±0.56	1.29±0.22	1.09±0.36
Unstimulated PMNs with unstimulated WM9 cells (3 cases)					
Global fitting	0.43	0.53*	2.06	0.46	0.91
Individual fitting	0.33±0.10	0.53†	1.60±0.46	0.61±0.16	0.24±0.21
fMLP-stimulated PMNs with TNF-α-stimulated WM9 cells (3 cases)					
1 U/ml	0.60	0.41†	3.52	1.84	1.83
10 U/ml	0.93	0.41†	6.16	0.43	0.49
100 U/ml	1.97	0.41†	14.52	0.14	1.01
fMLP-stimulated PMNs with unstimulated WM9 cells by blocking of β_2-integrin (3 cases)					
Global fitting	0.24	0.38*	0.91	0.82	4.75
Individual fitting	0.16±0.08	0.38†	0.61±0.28	0.90±0.11	0.83±0.48
fMLP-stimulated PMNs with unstimulated WM9 cells by blocking of ICAM-1 (4 cases)					
Global fitting	0.30	0.05*	1.18	2.00	1.84
Individual fitting	0.32±0.02	0.05†	1.24±0.03	2.03±0.32	0.29±0.25
Data from Ref. 23	0.70±0.15				
Data from Ref. 50	0.19–2.51				
Data from Ref. 8	1.28	0.41			

Four kinetic parameters were adjusted to describe the molecular mechanisms of polymorphonuclear neutrophil (PMN)-WM9 aggregation mediated by β_2-integrin and ICAM-1 in the model. Here k_r^0 is the zero-force reverse rate, a is the interaction range, $(A_c m_r m_l k_f)^0$ is the effective forward rate immediately after stimulation [time (t) = 0], and α is the decay factor describing the time dependence of the effective forward rate. Global fitting was done using a single parameter set [k_r^0, a, $(A_c m_r m_l k_f)^0$, and α] for 9 [formyl-methionyl-leucyl-phenylalanine (fMLP)-stimulated PMNs with unstimulated WM9 cells], 3 (unstimulated PMNs with unstimulated WM9 cells, β_2-integrin blocking), or 4 (ICAM-1 blocking) time courses in percentages of WM9 cells in heterotypic aggregation; the fitted parameters are presented. Individual fitting was performed by presetting the interaction range a obtained from the above global fitting and adjusting an individual parameter set [k_r^0, $(A_c m_r m_l k_f)^0$,

Am J Physiol Cell Physiol. Author manuscript; available in PMC 2009 May 7.

and *a*] for each case; the average values are presented as means ± SE. Data previously published were adopted for unstimulated PMNs in 5.0 mM Mg^{2+} plus EGTA (23), β_2-integrin locked in different conformations (50), and integrin $\alpha_4\beta_7$ interacting with mucosal addressin cell adhesion molecule-1 in the presence of 1.0 mM Ca^{2+} and 1.0 mM Mg^{2+} (8).

*Predicted interaction range *a* from global fitting

†preset interaction range *a* obtained from global fitting.

Am J Physiol Cell Physiol. Author manuscript; available in PMC 2009 May 7.